In press for 2027 Annual Reviews of Physiology

Vasomotion of Brain Arteries: Ionic Dynamics Through Systems Physiology in Health and Vascular Disease

Scott Earley[1], David Kleinfeld,[2] and Susanne J. van Veluw[3]

[1]Department of Pharmacology and Physiology, University of Rochester, Rochester, New York, USA; email: scott_earley@urmc.rochester.edu
[2]Departments of Physics and Neurobiology, University of California San Diego, La Jolla, California, USA; email:dk@physics.ucsd.edu
[3]BHF-UK DRI Centre for Vascular Dementia Research**,** Edinburgh, United Kingdom; email: susanne.vanveluw@ed.ac.uk

Abstract

The myogenic tone and thus diameter of brain arterioles varies on multiple time scales. These variations result from coordinated contraction and relaxation of electrically coupled smooth muscle cells in the arteriole wall that drive constriction. A prominent feature is a broad-band ~ 0.1 Hz rhythmicity, designated vasomotion, in the pial arterioles spanning the cortical mantle and the penetrating arterioles that nourish the capillary bed. As characterized in the murine brain, vasomotion supports propagating waves with a typical wavelength of 20 mm (speed of 2 mm/s) that modulate perfusion with a magnitude equal to that of functional hyperemia. The spectral and spatial properties reflect the interaction of smooth muscle dynamics with the underlying neuronal drive. Possible functional roles of vasomotion are to mitigate capillary stalls and to facilitate the exchange of solutes between interstitial and cerebrospinal fluid. Indeed, loss of vasomotion has been implicated in the pathophysiology of vascular disease, such as cerebral amyloid angiopathy.

INTRODUCTION

Vasomotion refers to the phenomenon of active vascular constriction and dilation that is driven by the smooth muscle cells (SMCs) that surround arteries and arterioles. While the designation is quite general, we specifically refer to the slow and somewhat irregular process that occurs about once every 10 seconds, or with a frequency centered around 0.1 Hz. This rate is 100-times less than the heart rate in mice and ten times less than the heart rate in human primates.

Our focus is rhythmic vasomotion in the brains of mammals. These rhythms are observed during wakefulness as well as non-REM (NREM) sleep. Current evidence indicates that vasomotion in brain arterioles is driven by mechanisms confined to lie within the brain(1). Yet, much as we have considerable knowledge about the phenomenology of brain vasomotion, the cellular mechanism of the oscillations remains an open challenge. Vasomotion in the brain can phase-lock, and unlock, with systemic oscillations that are close in frequency. This includes input from the heart and baroreceptor reflex, designated as Mayer waves in humans (2), or the peripheral vascular system (3-9).

PHENOMENOLOGY OF CORTICAL VASODYNAMICS

Long-Range Coherence of Oscillations

Vasomotion is a brain-wide phenomenon. The earliest data supporting this concept come from functional magnetic resonance imaging (fMRI) studies in humans (10). Here, the fMRI signals are based on inference from changes in blood oxygenation that is tied, albeit imperfectly, to the extent of deoxy- versus oxygenated blood and referred to as blood oxygenation level dependent (BOLD) fMRI. The pioneering study of Biswal and Hyde (11) showed that cortical regions that are mirrored across the two hemispheres show similar, concurrent activation under periods devoid of sensory simulation or motor acts. These so-called "resting state" signals occur across regions in which the underlying neurons are connected by long-range white matter connections, i.e., transcallosal projections in the case of interhemispheric signals (12). The results and interpretation of the fMRI studies are bolstered by the pioneering *in vivo* optical imaging studies of Mayhew (13) and subsequent fMRI (14-16) and additional optical studies (17-22); reviewed in (23-27).

Direct measurements in rodents support the view of transcallosal neuronal interactions enabling transhemispheric correlation in vessel diameter. Here, *in vivo* two-photon laser scanning

microscopy (TPLSM) was used to scan the diameter of individual vessels in mirrored transhemispheric locations using mice prepared with a thinned but intact skull (28) (**Figure 1a-c**). Notably, there are no common downstream arterioles that connect mirrored regions in the two hemispheres (29). Yet the mirrored regions show rhythmic vasodilations that are well synchronized, with a coherence near one (23) (**Figure 1c,d**).

The observation of long-range vasomotion synchrony at the vasomotion frequency leads to a model in which neuronal communication spanning the corpus collosum that links the two hemispheres will synchronize the ultraslow neuronal activity between mirrored regions. This in turn will partially entrain oscillations intrinsic to the vasculature, so that vasomotion across the mirrored regions is synchronous as well (23) (**Figure 1e**). This transhemispheric synchrony was attenuated but not eliminated in acallosal I/LnJ mice, implicating callosal pathways as a dominant substrate for bilateral coordination of vasomotion while leaving room for additional mechanisms. These oscillations, regardless of their origin, then drive oscillations in blood oxygenation that form the basis of changes in the BOLD fMRI signal (**Figure 1e**) or, equivalently, the intrinsic optical signal (IOS).

Irregular Rhythm

Vasomotion, as observed by a change in arteriolar diameter in healthy animals, is an irregular oscillation (23, 30) (**Figure 1c**). This means that the rhythm is not a pure sine wave, but rather one whose distribution of amplitudes for each spectral component has a maximum value or so-called center frequency near 0.1 Hz, with amplitudes that diminish both above and below this value over a half-width-half-maximum range of ~ 0.05 Hz. One possibility is that the underlying constrictive force generated by SMC actin in the arteriole walls is perfectly periodic, while the change in diameter is irregular because of fluctuations in the downstream hydrodynamic resistance. To test for this possibility, we can infer the nature of the drive to muscle constriction through a measurement of intracellular SMC Ca^{2+} (**Figure 1a,f**). More so, this measurement is performed concurrent with that of the diameter of the vessels (31). We find that the spectral distribution is broad for the measurement of SMC Ca^{2+} just as it was for diameter, and essentially unchanged over time (**Figure 1f-h**). We conclude that irregular oscillations are a fundamental aspect of vasomotion.

A final point is that despite the wide bandwidth of the vasomotion oscillation, the center frequency of the activity is well defined. The center frequency is stable over periods of hundreds

to thousands of seconds (**Figure 1f-h**). Yet, over a large cohort of murine individuals and separate trials, the center frequency spanned the range 0.02 to 0.16 Hz. This distribution is neither normal nor uniform; there is a peak at 0.11 Hz with a half-width-half-maximum of 0.02 Hz, and a broad shoulder extending down to 0.01 Hz, the limit of these measurements (30) (**Figure 1i**).

Why Is the Spectrum of vasomotion So Broad?

One way to view the spectrum is as a mixture of multiple frequencies. A hint for the utility of such dynamics comes from comparison with another slowly oscillating system - the gut. In the gut, isolated segments have relatively pure oscillations with a single frequency (32, 33). Plus, there is a natural shift in the frequency of isolated segments, with segments at the level of the stomach higher in frequency than those toward the rectum. In the intact system, the frequency gradient is replaced by a staircase of segments of the gut, with a decreasing frequency down the staircase. This leads to a traveling wave from stomach to rectum as well as to a pinch-off in the diameter of the gut at the boundary between segments. Pinch-off leads to a "chain of sausages" that allows food to be churned and mechanically digested. Numerical solution of associated neuronal equations confirms this behavior (34, 35), while the analytical solution of coupled oscillator dynamics provides insight into the generality of the pinch-off (36).

In the bloodstream, pinch-off, or so-called "sausage-string" vessels are reportedly observed in radiological images from human brains (37) and documented for pial arterioles of cynomolgus monkeys made hypertensive by renal ischemia (38). While vasomotion was not recorded, we note that the stroke prone spontaneously hypertensive rat is known to exhibit endogenous, almost perfectly sinusoid oscillation (39). We thus speculate that brain arterioles in healthy animals exhibit broad-band oscillations to avoid diminution of blood flow by pinch-off.

Is Vasomotion Autonomous?

Ex vivo preparations of pial and penetrating arterioles from healthy, wild-type animals do not show oscillations. Vasomotion oscillations, with a relatively pure frequency, occur for the aforementioned special case of hypertensive vessels or under pharmacological manipulation (39, 40). Brain arterioles are readily entrained to ongoing or sensory-induced neuronal activity in the 0 to 0.2 Hz range (31). What is the source of ultra-low ~ 0.1 Hz neuronal electrical activity in the brain that can lock to or entrain the 0.1 Hz vasomotion activity? Measurements from humans (41), non-human primates (42, 43), and rodents (23) show that ultra-low frequency electrical activity originates as a modulation in the spectral power of the high-frequency gamma-oscillations. This

collective, ongoing activity overlaps with the natural frequency of the vessel response - either active or passive. General theories of coupled oscillators imply that the two systems will phase-lock, if their frequencies are close, for a sufficiently strong interaction (44). The details of their interaction determine the particular phase shift.

Oscillations Correspond to Long-Wavelength Propagating Waves

So far, we have considered activity at either a single arteriole (**Figure 1f-h**) or at pairs of arterioles mirrored across cortical hemispheres (**Figure 1b-d**). At the scale of the cortical mantle, we find that the oscillations show continuous if noisy phase-shifts that correspond to waves of varying wavelength, but typically on the order of 20 mm, equal to the entire extent of the cortical mantle. The variability in phase can be extracted from full field images of the $[Ca^{2+}]$ in arterioles that express SMC actin (30, 45). In the example 1 of **Figure 1j**, vasomotion waves travel on a lateral-to-medial and rostral-to-caudal axis on average. The relation of rhythmic frequency to spatial phase shift, which is proportional to the spatial frequency of the traveling waves, leads to an estimate wave speed of 2 mm/s (30). This corresponds to the extracted speed for communication of electrical signaling along capillary endothelial cells in mouse (46). We envision the network as an arteriole with SMC oscillators that interact through their gap-junction connections with the similarly electronically connected endothelial cells that form the lumen of the arteriole (**Figure 1k**). Verification would involve a means to reversibly interrupt gap junction communication, perhaps with tools based on specific subtypes of connexins in endothelial cells (47).

What of the penetrating arterioles? Here, detailed measurements of the diameter along the length of penetrating arterioles show that they too support traveling waves (30), albeit phase shifts are relatively small as the thickness of cortex, ~ 1 mm, is much less than one wavelength, ~ 20 mm. The directions of the waves appear to be random from arteriole to arteriole. Thus, penetrating arterioles are compressing and relaxing the parenchyma in the cortex, which will mix solutes, but the absence of coherent movement is unlikely to provide a field for the non-displacement of solutes.

The available evidence, therefore, points to ultra-low frequency modulation of neuronal gamma-band power as the principal driver of cortical vasomotion. This can be enhanced by sensory stimulation. The remaining challenge is to define the vascular signaling architecture that converts this activity into rhythmic changes in arteriole tone and diameter.

Correlative and Causal Impact of Neuronal Activity

We consider the temporal variation in the spectral power of the LFP in the upper layers of cortex in relation to changes in the diameter of the surface arterioles (**Figure 2b**). The field potential shows epochs of enhanced electrical activity across all frequency bands, yet variations in power are greatest in γ-band and are broadly distributed with a periodicity near 0.1 Hz. Crucially, changes in the diameter of surface arterioles co-vary with the power in the $\gamma-$band (**Figure 2a**). The timing of the fluctuations is such that the electrical activity leads that of the diameter by ~ 2 s. More so, the direction of propagation of the vasomotion traveling wave is biased by the propagation of the underlying electrical activity, such that the choice of direction has a small but significant correlation of about 0.3 (**Figure 2b**). Sensory activity, such as through stimulation of the vibrissae, barely changes the correlation of vasomotion and the ongoing neuronal activity (**Figure 2c**). When optogenetic excitation is used to drive pyramidal neurons, we see that the induced peak in the gamma rhythm power leads the increase in vessel diameter (**Figure 1d**). In contrast, using optogenetic inhibition of arterioles to drive their dilation does not impact neuronal activity (23). These experiments add to the long-range correlation measurements and confirm the neurovascular coupling scheme of **Figure 1e**.

PHYSIOLOGY OF CORTICAL VASODYNAMICS

We now examine how neuronal activity is linked to vasomotion at the level of capillaries, endothelial cells, and arteriolar SMCs in the brain. Rhythmic contractile activity can occur in other organs, but the frequency distribution and underlying mechanisms differ from arteriolar diameter oscillations in the brain. The portal vein is a classic model for spontaneous rhythmic smooth-muscle activity, although this behavior is more commonly described as spontaneous rhythmic contraction, slow-wave activity, or peristalsis rather than vasomotion in the arteriolar sense (48). The portal vein is unusual among blood vessels because it contains a prominent longitudinal smooth-muscle layer and exhibits phasic smooth-muscle behavior that is more reminiscent of gut or bladder than of resistance arteries. Accordingly, isolated portal veins generate spontaneous bursts of action potentials associated with rhythmic contractions. By contrast, arterial SMCs do not fire action potentials under physiological conditions, except when damaged or experimentally manipulated to disrupt normal membrane-potential regulation.

The focus here is therefore on the particular cellular and ionic mechanisms that govern arteriolar dynamics in the brain, with particular emphasis on neuronal activity detection and

intercellular electrical conduction pathways through which signals arising in the capillary bed are transmitted to upstream resistance vessels. Together, these processes provide the mechanistic framework for coupling changes in membrane potential, intracellular Ca^{2+}, and contractility to generate rhythmic diameter oscillations.

Setting the Tone

The dilator component of vasomotion results from coordinated relaxation of electrically coupled arterial SMCs in the vessel wall. Graded changes in SMC membrane potential (E_M) and intracellular [Ca^{2+}] drive changes in contractility and diameter (49) (**Figure 3a-c**). Depolarization increases Ca^{2+} influx through voltage-dependent $Ca_V1.2$ channels and promotes constriction; hyperpolarization has the opposite effect. Under physiological pressures, SMCs sit in a partially depolarized state that sustains steady-state myogenic tone, and this baseline excitability is continuously tuned by additional inputs, such as endothelium-derived signals, circulating factors, perivascular neurons, astrocytes, microglia, and local metabolites, that nudge E_M, SMC [Ca^{2+}], and luminal diameter to appropriately match tissue demand or other situational requirements. The steep voltage dependence of $Ca_V1.2$ gating (50) imparts exquisite sensitivity, and a shift of a few millivolts in E_M produces disproportionately large changes in SMC [Ca^{2+}] and diameter (49). Based on simplified transfer functions relating SMC E_M, intracellular Ca^{2+}, and arterial diameter from **Figure 3a-c** and the empirical data of Knot and Nelson (49), a 20% dilation is estimated to require only ~ 5 mV of hyperpolarization and an accompanying ~ 30 nM decrease in global intracellular Ca^{2+}. As a result, arterial SMCs can be viewed as high-gain amplifiers, converting subtle electrical signals into meaningful changes in diameter. Importantly, diameter changes during vasomotion are phase-locked to oscillations in SMC [Ca^{2+}] (30) (**Figure 2a**), providing strong evidence that this process is driven by corresponding electrical signals.

What Sets the Electrical Rhythm In Vivo?

A key consideration arises from a large body of literature showing that vasomotion in the 0.1-Hz range is rarely observed in isolated, pressurized cerebral arteries studied *ex vivo* using standard pressure myography techniques (51). Instead, when pressurized to a physiological range, e.g., 40–80 mmHg, cannulated cerebral pial arteries and arterioles typically develop stable SMC E_M and corresponding levels of myogenic tone (49). Diameter changes under these conditions can be evoked by pharmacologic interventions acting directly on SMCs or indirectly via the endothelium (**Figure 3f**). The few studies reporting arterial oscillations *ex vivo* are typically

contingent on special circumstances, such as the use of arterioles from stroke-prone hypertensive rats (39) or on specific perturbations, such as the addition of potassium channel blockers, and may occur at frequencies that do not match the ~ 0.1-Hz band (39, 52). This disparity indicates that the *in vivo* rhythm depends on hyperpolarizing electrical inputs that are amputated during pressure myography and is not driven by innate pace-maker processes normally active at the level of SMCs or the endothelium. Missing elements that could provide the appropriate input *in vivo* include an electrically coupled capillary network with associated pericytes and the brain's ongoing neuronal activity.

Capillaries Catch the Wave

Arterial SMCs provide system gain, translating small voltage perturbations into disproportionately large changes in Ca^{2+} and diameter. However, the absence of corresponding ultra-low frequency oscillations in isolated and pressurized cerebral vessels indicates that the mural cell machinery is not, by itself, sufficient to generate vasomotion under normal physiological conditions. This observation shifts attention to the broader neurovascular unit, particularly to the brain's enormous, electrically continuous capillary network, a structure that is ideally positioned to receive and filter ongoing neuronal activity and transmit this information to upstream vascular segments. Compelling evidence that capillaries act as sentinels of brain activity came from Longden et al. (46), who showed that inwardly rectifying K^+ ($K_{ir}2.1$) channels in capillary endothelial cells sense modest increases in extracellular K^+ released by active neurons and generate retrograde hyperpolarizing signals that relax upstream SMCs and dilate arterioles, thereby producing functional hyperemia (46, 53). This concept is illustrated by experiments shown in **Figure 3d-f**. Parenchymal arterioles can be isolated from brain slices with intact capillary beds, mounted in pressure myography chambers, and, after the spontaneous myogenic tone develops, imaged *ex vivo* (**Figure 3d,e**) as pulses of K^+ (~ 10 mM) are pico-ejected onto the capillary segments. This intervention causes robust and reproducible conducted dilation of upstream arterioles (**Figure 3f**). Subsequent studies demonstrated that activation of transient receptor ankyrin 1 (TRPA1) cation channels (54) and prostaglandin E(2) (PGE_2) receptors (55) with appropriate agonists can also orchestrate this response. This capillary-to-arteriole signaling mechanism is now recognized as a fundamental component of neurovascular coupling (56).

Inward rectifying K^+ channels are particularly well suited for this sensory role because their activity increases at negative membrane potentials and can therefore reinforce and propagate

hyperpolarizing signals through the capillary syncytium (46, 53). Consequently, the capillary network architecture provides two essential properties for converting gamma-band neuronal activity into an ultra-low frequency vasomotion rhythm. First, it provides nonlinear gain, i.e., modest increases in local extracellular [K^+] can amplify changes in endothelial cell E_M through the unique voltage- and [K^+]-dependent activation properties of K_{ir}2.1 channels (46). These changes in E_M are transmitted to overlying SMCs via myoendothelial gap junctions to cause vasodilation. Second, it provides spatial and temporal integration, i.e., in principle, the capillary bed samples neuronal activity over the entire brain, averaging over local variability in spiking activity and generating a coherent territory-level signal. These observations are bolstered by computational analyses that further suggest that the capillary network behaves as a nonlinear electrical sensor and amplifier, allowing small inputs to evoke disproportionately large vasodilatory responses (53). In the case of brain-wide gamma-band activity, extracellular K^+ dynamics are already low-pass filtered by diffusion, buffering, and mixing, and the capillary network imposes an additional layer of spatial averaging and electrical integration. Together, these processes enable the capillary bed to function as a biological gamma-band envelope receiver, transforming structured high-frequency neuronal activity into slowly varying endothelial and SMC voltage signals, thereby driving the dilator component of vasomotion.

The extracellular K^+ hypothesis predicts that if capillary K_{ir}2.1 channels serve as the primary demodulator, then pharmacologic inhibition or endothelial cell-specific genetic deletion of the channel should reduce the coherence and spectral prominence of ~ 0.1 Hz vasomotion, while preserving or enhancing basal myogenic tone. Likewise, perturbations that alter extracellular handling of K^+, such as ablating astrocytic K_{ir}4.1 or Na^+/K^+-ATPase activity, should shift the center frequency, stability, or spatial coherence of the rhythm by changing the kinetics of extracellular K^+ accumulation and clearance. This framework does not exclude contributions from other capillary signals, including the generally much slower purinergic pathways, metabolic cues, or pericyte-derived electrical influences, but it places K_{ir}-mediated capillary conduction at the center of the frequency-transforming step. These observations support a phenomenological model in which an ultra-low frequency gamma-band envelope drives a nonlinear capillary K_{ir} amplifier that modulates upstream SMC E_M, which is converted to intracellular Ca^{2+} and diameter changes using empirically derived sigmoidal transfer functions to produce the dilation component of the vasomotion process (**Figure 3g**). However, the Longden et al. (46) and Moshkforoush et al. (53) framework is fundamentally vasodilatory and does not explain the vasoconstrictive component of

arteriole vasomotion. Experimental evidence suggests that vasoconstriction following a single, transient K_{ir} channel-mediated hyperpolarizing signal most likely reflects restoration of basal myogenic tone (**Figure 3f**).

IMPLICATIONS OF VASOMOTION IN NORMAL PHYSIOLOGY AND DISEASE

What Is the Purpose of Vasomotion?

Despite the renewed interest and growing literature on vasomotion, its exact role in the brain is incompletely understood (57). In this section, we provide a few thoughts on possible physiological functions of vasomotion.

Prevention of capillary stalls. The capillary network in the brain consists of narrow vessels in which red blood cells (RBCs) proceed in single file through vessels that meet as triadic nodes (58). At any moment, blood flows in the vast majority capillary branches, i.e., only 0.4 % of capillaries are stalled in normal animals yet substantially more in the APP/PS1 and 5xFAD mouse models of Alzheimer's pathology (1.8 %) (59). This extent of perfusion in normal mice appears remarkable, as one qualitatively expects a capillary network to have some branches with negligibly small pressure differences. While flow in the capillary network largely follows linear hydrodynamic equations, there is a minimum speed to capillary flow in mice, i.e., ~ 0.02 mm/s (60). This minimum speed is a factor of 50-times less than the typical flow speed. We hypothesize that the capillaries with stalled RBCs have pressure differences that drop below a minimum level that will sustain flow of RBCs, and asked if vasomotion can alleviate stalls. Vasomotion leads to changes in perfusion of about 20 % on a per cycle basis in mouse (30). Noting that the mean distance between penetrating arterioles is ~ 0.2 mm (61), or 100-times less than the typical wavelength of vasomotion waves (30), we could expect that vasomotion leads to shifts of 0.2 % in pressure across a capillary territory that is sufficient, albeit just barely so, to drive a stalled RBC past the threshold speed. This hypothesis gains credence from the observation that many stalls tend to last for only ~ 10 s (62), consistent with vasomotion fluctuations. This mechanism, if confirmed experimentally, bears on transient hypoxia (63) and cognitive decline (59, 64) in the face of impaired vasomotion. It complements changes in capillary hydrodynamics resistance caused by ensheathing pericytes (65-67).

Cerebrospinal and interstitial fluid movement. Accumulating evidence suggests that vasomotion may facilitate the movement of cerebrospinal fluid (CSF) and interstitial fluid (ISF), resulting in the clearance of solutes from the brain (68-70). Specifically, vasomotion has been postulated to drive fluid transport along perivascular compartments where CSF exchanges with ISF, thereby promoting the efflux of soluble, e.g., metabolic waste, products (71) (**Figure 4**). The overarching idea is that dilation of the arteriole walls will lead to net movement of solutes in the ISF and permit them to be drained by transport through perivascular compartments. This implies that there is a mechanism to break the bidirectional movement of solutes and/or a mechanism to absorb soluble products, such as amyloid-β, that have moved to a downstream target.

Although insights from computational modeling studies remain inconclusive with regard to the individual physiological driving forces of CSF-ISF exchange (70), ultra-low frequency arteriolar oscillations have emerged as a likely candidate (72, 73). This conclusion follows from the shorter wavelength of vasomotion compared to cardiac pulsations in the brain (72), and the low-pass nature of pial arterioles, whose vaso-elastic compliance leads to a cut-off frequency of ~ 0.22 Hz in mice (30). Indeed, when perivascular clearance pathways were modeled as poroelastic tissue materials, vasomotion was predicted to induce a net volume flow rate (74), notably owing to the asymmetry of the arteriolar oscillations during functional hyperemia (45, 75, 76).

It is possible that there is no mechanism that results in advection, i.e., directed flow. Nonetheless, even in the absence of a net volume flow rate, dissolved or even suspended proteins in the CSF and ISF will spread because of diffusion, with a net excursion that increases as distance $\propto \sqrt{\text{time}}$ rather than distance $\propto$ time in the presence of a convective field. Yet any movement of brain compartments because of expansion of tissues, as occurs with vasomotion of arterioles (30, 45), changes in water balance or volume between compartments (77), can lead to sloshing and mixing of CSF and ISF that exceeds the excursion from diffusion. This model is analogous to the churning of clothes in a washing machine (78). Indeed, recent work in rodents shows that peristaltic vasomotor waves in neighboring penetrating arterioles move both inward and outward without apparent order (30), supporting the idea of mixing rather than advection. For either mixing or advection to be effective, the excursions of the dissolved or suspended proteins in the CSF and ISF must extend to clearance routes among proximal borders in the brain (79-85) as unambiguously observed using endogenously expressed tracer proteins (86). Of course, for either mixing or advection, an increase in vasomotion would increase clearance (87, 88).

Evidence that vasomotion may be a facilitator of CSF and ISF movement. Experimental evidence supporting the hypothesis that vasomotion may be a facilitator of CSF and ISF movement is mainly derived from studies with mice that rely on the delivery of tracers directly into the CSF, e.g., intra-cisternal or ISF compartments via intra-parenchymal delivery, although the field is moving towards developing novel non-invasive tracing methods (86) (**Sidebar 1**). Initial observations suggested that tracer movement was coupled to cardiac pulsatility (83, 89). However, the imaging parameters in these studies did not capture ultra-low frequency vessel oscillations, and they were performed under anesthesia, which can diminish vasomotion. In a subsequent *in vivo* TPLSM imaging experiment, vasomotion was recorded in head-fixed unanesthetized awake mice and found to be correlated with the loss of signal amplitude from a fluorescent tracer surrounding pial surface arterioles in the subarachnoid space (87) (**Figure 4f-h**). Moreover, during 0.05 Hz visual stimulation with an alternating checkerboard pattern that rapidly flickered (8 Hz), tracer cleared faster than under the absence of visual stimulation (grey screen). This result was interpreted to be the consequence of greater oscillation amplitude induced by functional hyperemia during visual stimulation (**Figure 4a-e**). As an additional control, administration of isoflurane anesthesia, which is a potent vasodilator (90), resulted in a complete loss of vasomotion, as well as response to visual stimulation, and was associated with slower tracer clearance rates (87). A subsequent study similarly found that functional hyperemia in response to 0.017 Hz vibrissa stimulation in ketamine/xylazine anesthetized mice that received intra-cisternal injections of fluorescent tracers led to both an increased tracer signal influx as well as tracer efflux (91) (**Figure 4i,j**). Furthermore, using SM22-Cre:Ai32-ChR2 mice, optogenetic stimulation over a 30-minute recording period and targeted to the vascular SMCs of the middle cerebral artery resulted in an increase of tracer signal influx compared to the unstimulated hemisphere (91). In total, these findings suggest that the rhythmic slow oscillations of brain arterioles are sufficient to facilitate fluid movement in the brain and that augmenting vasomotion through functional hyperemia may increase CSF-ISF exchange. More so, vagus nerve stimulation (92) and NREM sleep (88, 93, 94), albeit these latter claims are controversial (95), may further augment CSF-ISF exchange.

Evidence from Human imaging

The development of non-invasive MRI sequences enabled the relationship between ultra-low frequency vascular oscillations and CSF movement in the human brain to be studied (96). In an in vivo 3 tesla BOLD fMRI study that used young healthy volunteers during nighttime sleep, large

oscillations in an MRI signal indicative of CSF flow within the fourth ventricle were coupled with ~ 0.05 Hz BOLD oscillations in the cortical gray matter during NREM sleep (97). These temporally coupled CSF-BOLD oscillations were strongly anticorrelated. Of note, slow delta neuronal waves, as measured with EEG, were found to precede CSF waves by ~ 6.4 s (97). These findings demonstrate that ultra-low frequency oscillations in neuronal activity, blood, and CSF flow are tightly coupled in the human brain, in line with the Monro-Kellie doctrine, which dictates that – due to the rigid skull and fixed intracranial volume – any increase in brain tissue or blood volume will necessarily require a decrease in CSF to maintain normal intracranial pressure. Ongoing developments in the field are now starting to generate the first measurements of CSF flow within the smaller perivascular spaces of the human brain. A recent study introduced a 0.45 mm isotropic voxel resolution *in vivo* 7 tesla MRI sequence with T2-preparation to isolate the CSF signal in the human brain and motion-sensitizing gradients of 3.5 mm/s to calculate tensors. This method, termed CSF-STREAM, realizes quantitative measurements of CSF mobility within the subarachnoid spaces as well as the perivascular spaces surrounding individual arterioles in the human brain (98). Both cardiac pulsations as well as respiration were associated with CSF mobility in perivascular spaces, although cardiac pulsations were associated with larger CSF mobility oscillations in the larger CSF spaces, e.g., the fourth ventricle and the subarachnoid space around the middle cerebral artery, compared to respiration. Of note, driving vasomotion with a 0.1 Hz visual stimulation paradigm increased CSF mobility in the occipital cortex, although the effect was modest, i.e., 1.2 % on average (98).

Whether vasomotion is implicated in the removal of soluble proteins typically associated with neurodegenerative disorders, e.g., amyloid-β and tau, remains experimentally unresolved (**Box 1**). Likewise, it is not clear whether enhancing vasomotion, e.g., using optogenetic stimulation, functional hyperemia, hypercapnia, sleep, or vagus nerve stimulation could promote clearance of these substances, although a recent study was suggestive of increased protein clearance after a period of intermittent hypercapnia (99).

Vasomotion is decreased in cerebral amyloid angiopathy. Impaired vasomotion has been implicated in cerebral amyloid angiopathy (CAA) – one of the most common forms of cerebral small vessel disease and a major cause of microvascular brain injury and hemorrhagic stroke (100). Cerebral amyloid angiopathy is characterized by the deposition of amyloid-β in the walls of pial surface vessels, penetrating arterioles, and the capillaries (101). The gradual accumulation of vascular amyloid-β coincides with a loss of SMC contractility, thereby resulting in reduced

vascular compliance (102, 103). Indeed, impaired vascular reactivity as measured with BOLD fMRI in response to a visual stimulation has been observed in patients with sporadic CAA (104, 105) as well as individuals with hereditary Dutch-type CAA, as early as in pre-symptomatic mutation carriers (106). Interestingly, the 5xFAD mouse model exhibits diminished neurovascular coupling due to dysfunction of endothelial $K_{ir}2.1$ channels (107). Our model predicts that this defect would also impair vasomotion. A gradual loss of vasomotion was observed in the APP23 mouse model that exhibits CAA, coinciding with the gradual accumulation of amyloid-β in pial arterioles (108). Furthermore, impaired vasomotion in mouse models with CAA has been found to be associated with reduced tracer clearance (87, 109). Notably, in patients with CAA a 20 % increase in CSF mobility was found in the subarachnoid space immediately adjacent to the middle cerebral artery, compared to age-matched controls (98), but not the perivascular spaces in the brain. These initial observations of altered CSF dynamics in the context of CAA are in line with previous findings of altered tracer dynamics injected into the CSF in rats with CAA (110) and suggest a disruption in the efficiency of CSF-ISF exchange.

Vasomotion and amyloid-β. An essential concept linking vasomotion and health is that amyloid-β, which is mainly produced in the cortical parenchyma, ends up in the vessel wall because of impaired clearance, either through a reduction of effective enzymatic degradation, failed transport across the blood-brain barrier, or via ISF drainage routes. Initial amyloid-β depositions in the vessel wall may act as “sticky seeds” that can induce subsequent accumulation along the vasculature in a propagating fashion (111). This results in a feed-forward detrimental cycle of further loss of SMC contractility, thickening of the vessel wall, extracellular matrix remodeling, and most likely obstruction of the perivascular compartments, thereby negatively impacting CSF-ISF exchange and solute clearance. Whether any of these pathophysiological processes are reversible remains unclear. Future studies are needed to determine whether entraining vasomotion in the context of CAA can effectively enhance CSF-ISF exchange and promote amyloid-β drainage.

EPILOGUE

Vasomotion is intrinsic to the vessels in the brain, but, like all oscillators, vasomotion can lock, and unlock, with a multitude of systemic oscillators throughout the body. The overall spatial pattern of vasomotion in the brain is largely fixed, even when locked in part to an external stimulus.

A fast mechanism for partial locking of vasomotion to neuronal activity is through electrical communications from neurons to capillaries to arterioles. This can be altered by neuromodulators and impacted by vascular disease. One critical future direction is the development of a Hodgkin-Huxley-like analysis of coupled smooth muscle cells. Another is a clearly defined role, if any, for vasomotion in clearance of soluble waste products generated in the brain, how vasomotion is compromised in pathologies, such as CAA, and how we can modulate vasomotion to improve clearance.

Disclosure statement

The authors have no commercial interests.

Acknowledgments

We thank Patrick Drew, Jacob Duckworth, Luke Kaplan, Leon Munting and Massimo Vergassola for discussions. This work was funded by the United States National Institutes of Health grants R35 HL155008 to S.E. and R35 NS097265 and U19 NS137920 to D.K., and the Leducq Foundation for cardiovascular research grant 23CVD03 to S.v.V. This work was further supported by the UK Dementia Research Institute [Group Leader Award – BHF-UK DRI Centre for Vascular Dementia Research to S.v.V.] through UK DRI Ltd, principally funded by the Medical Research Council.

SIDEBAR: Technical Considerations Regarding In Vivo Imaging of Vasomotion and CSF-ISF Exchange

- Surgical preparations: cranial windows are often required to gain optical access to the cerebrovasculature. Open craniotomies may diminish vasomotion, even after closure and especially in the acute phase. Thin skull windows are recommended (112, 113), which are more likely to preserve vasomotion in vivo.
- Anesthesia: certain anesthetics may alter vasomotion and CSF-ISF exchange (114).
- Contamination or misattribution of signal: although vasomotion is most readily observed in habituated head-fixed unanesthetized mice, confounding variables that can influence vasomotion in this condition should be considered, such as movement associated with locomotion, twitching, and fidgeting (18, 25, 115).
- Tracer injections: current study of CSF-ISF exchange relies on injection of tracers into CSF or ISF compartments. This can induce artefacts from the added volume and pressure-induced flow. Recall that 1 nL of solution is equivalent to a sphere of 90 μm in radius, or a sphere of 160 μm in radius for injection into the interstitial space of brain tissue (116). Further, a typical 10 μL infusion into a ventricle (117) must be compared to the 50 μL total ventricular volume in a mouse (118). A notable exception is to trace clearance of fluorescently tagged neuron-derived and extruded proteins (86).
- Human studies: there is a need to advance and adopt methods for single-vessel resolution with human MRI (119, 120).

Literature cited

1. Alzetani A, Duckworth J, Birch AA, Simpson DM, Kleinfeld D, Carare RO. 2026. Ultralow frequency vaso-oscillations in human cerebral arteries are independent from Mayer waves. *bioRxiv* BIORXIV/2026/731141
2. Julien C. 2006. The enigma of Mayer waves: facts and models. *Cardiovascular Research* 70: 12-21
3. Diehl RR, Diehl B, Sitzer M, Hennerici M. 1991. Spontaneous oscillations in cerebral blood flow velocity in normal humans and in patients with carotid artery disease. *Neuroscience Letters* 127: 5-8
4. Quirk K, Ladrón-de-Guevara A, Raghunandan A, Mestre H, Nedergaard M, Kelley DH. 2026. Quantifying cerebrospinal fluid flow in pial perivascular spaces of rats. *Fluids and Barriers of the CNS* 23: 41-
5. Willie CK, Tzeng Y, Fisher JA, Ainslie PN. 2014. Integrative regulation of human brain blood flow. *Journal of Physiology* 592: 841-59
6. Hablitz LM, Vinitsky HS, Sun Q, Stæger FF, Sigurdsson B, et al. 2019. Increased glymphatic influx is correlated with high EEG delta power and low heart rate in mice under anesthesia. *Science Advances* 5: eaav5447
7. Bolt T, Wang S, Nomi JS, Setton R, Gold BP, et al. 2024. Autonomic physiological coupling of the global fMRI signal. *Nature Neuroscience* 28: 1327–35
8. Claassen JAHR, Levine BD, Zhang R. 2009. Dynamic cerebral autoregulation during repeated squat-stand maneuvers. *Journal of Applied physiology* 106: 153–60
9. Lachert P, Zygierewicz J, Janusek D, Pulawsk P, Sawosz P, et al. 2019. Causal coupling between electrophysiological signals, cerebral hemodynamics and systemic blood supply oscillations in Mayer wave frequency range. *International Journal of Neural Systems* 29: e1850033
10. Ogawa S, Tank DW, Menon R, Ellermann JM, Kim S-G, et al. 1992. Intrinsic signal changes accompanying sensory stimulation: Functional brain mapping with magnetic resonance imaging. *Proceedings of the National Academy of Sciences USA* 89: 5951-55
11. Biswal B, Yetkin FZ, Haughton VM, Hyde JS. 1995. Functional connectivity in the motor cortex of resting human brain using echo-planar MRI. *Magnetic Resonance in Medicine* 34: 537-41
12. Fox MD, Raichle ME. 2007. Spontaneous fluctuations in brain activity observed with functional magnetic resonance imaging. *Nature Reviews of Neuroscience* 8: 700-11
13. Mayhew JEW, Askew S, Zeng Y, Porrill J, Westby GWM, et al. 1996. Cerebral vasomotion: 0.1 Hz oscillation in reflectance imaging of neural activity. *NeuroImage* 4: 183-93
14. Xiong J, Parsons LM, Gao JH, Fox PT. 1999. Interregional connectivity to primary motor cortex revealed using MRI resting state images. *Human Brain Mapping* 8: 151–56
15. Fox MD, Corbetta M, Snyder AZ, Vincent JL, Raichle ME. 2006. Spontaneous neuronal activity distinguishes human dorsal and ventral attention systems. *Proceedings of the National Academy of Sciences USA* 103: 10046-51
16. Zhang Y-Y, Li J-Z, Wang W-T, Xie H-Q, Ruan J-Y, Jia J-M. 2025. Vasomotion delineates cerebral vascular dynamic features and participates in the homeostatic cerebral blood flow regulation. *Scientific Reports* 15: e36210
17. Ma Y, Shaik MA, Kozberg MG, Kim SH, Portes JP, et al. 2016. Resting-state hemodynamics are spatiotemporally coupled to synchronized and symmetric neural activity in excitatory neurons. *Proceedings of the National Academy of Sciences USA* 113: 8463-71
18. Drew PJ, Mateo C, Turner KL, Yu X, Kleinfeld D. 2020. Ultra-slow oscillations in fMRI and resting state connectivity: Neuronal and vascular contributions and technical confounds. *Neuron* 107: 782-804

19. Bruyns-Haylett M, Harris S, Boorman L, Zheng Y, Berwick J, Jones M. 2013. The resting-state neurovascular coupling relationship: Rapid changes in spontaneous neural activity in the somatosensory cortex are associated with haemodynamic fluctuations that resemble stimulus-evoked haemodynamics. *European Journal of Neuroscience* 38: 2902-16
20. Chan AW, Mohajerani MH, LeDue JW, Wang YT, Murphy TH. 2015. Mesoscale infraslow spontaneous membrane potential fluctuations recapitulate high-frequency activity cortical motifs. *Nature Communications* 6: 7738
21. Obrig H, Neufang M, Wenzel R, Kohl M, Steinbrink J, et al. 2000. Spontaneous low frequency oscillations of cerebral hemodynamics and metabolism in human adults. *NeuroImage* 12: 623–39
22. Winder AT, Echagarruga C, Zhang Q, Drew PJ. 2017. Weak correlations between hemodynamic signals and ongoing neural activity during the resting state. *Nature Neuroscience* 20: 1761–69
23. Mateo C, Knutsen PM, Tsai PS, Shih AY, Kleinfeld D. 2017. Entrainment of arteriole vasomotor fluctuations by neural activity is a basis of blood oxygen level dependent "resting state" connectivity. *Neuron* 96: 936-48
24. Aalkjaer C, Nilsson H. 2005. Vasomotion: Cellular background for the oscillator and for the synchronization of smooth muscle cells. *British Journal of Pharmacology* 144: 605–16
25. Drew PJ, Winder AT, Zhang Q. 2019. Twitches, blinks, and fidgets: Important generators of ongoing neural activity. *The Neuroscientist* 25: 298–313
26. Duyn J. 2011. Spontaneous fMRI activity during resting wakefulness and sleep. *Progress in Brain Research* 193: 295-305
27. Meyer-Baese L, Jaeger D, Keilholz S. 2025. Neurovascular coupling: a review of spontaneous neocortical dynamics linking neuronal activity to hemodynamics and what we have learned from the rodent brain. *Journal of Neurophysiology* 133: 644-60
28. Tsai PS, Mateo C, Field JJ, Schaffer CB, Anderson ME, Kleinfeld D. 2015. Ultra–large field-of-view two-photon laser scanning microscopy. *Optics Express* 23: 13833-47
29. Ji X, Ferreira T, Friedman B, Liu R, Liechty H, et al. 2021. The brain microvasculature has a common topology with local differences in geometry that match metabolic load. *Neuron* 109: 1168-87
30. Broggini T, Duckworth J, Ji X, Liu R, Xia X, et al. 2024. Long-wavelength traveling waves of vasomotion modulate the perfusion of cortex. *Neuron* 112: 2349-67
31. Duckworth J, Broggini T, Chhabria K, Neill P, Sellier-Prono M, et al. 2026. Arteriole mechanoresonances across the cortical mantle are shaped by competition among driven and resting-state vaso-oscillations. *Submitted*
32. Diamant NE, Borto A. 1969. Nature of the intestinal low-wave frequency gradient *American Journal of Physiology - Regulatory, Integrative and Comparative Physiology* 216: 301-07
33. Diamant NE, Bortoff A. 1969. Effects of transection on the intestinal slow-wave frequency gradient. *American Journal of Physiology - Regulatory, Integrative and Comparative Physiology* 216: 734-43
34. Patton RJ, Linkens DA. 1978. Hodgkin-Huxley type electronic modelling of gastrointestinal electrical activity. *Medical and Biological Engineering and Computing* 18: 195-202
35. Parsons SP, Huizinga JD. 2020. Modulation of contractions in the small intestine indicate desynchronization via supercritical Andronov–Hopf bifurcation. *Scientific Reports* 10: e15099
36. Sellier-Prono M, Cencini M, Kleinfeld D, Vergassola M. 2025. Defects, parcellation, and renormalized negative diffusivities in non-homogeneous oscillatory media. *Physical Review Letters* 135: e168401
37. Ducros A, Boukobza M, Porcher R, Sarov M, Valade D, Bousser M-G. 2007. The clinical and radiological spectrum of reversible cerebral vasoconstriction syndrome. A prospective series of 67 patients. *Brain* 130: 3091-101

38. Rodda R, Denny-Brown D. 1966. The cerebral arterioles in experimental hypertension. I. The nature of arteriole constriction and its effects on the collateral circulation. *American Journal of Pathology* 49: 53-76
39. Osol G, Halpern W. 1988. Spontaneous vasomotion in pressurized cerebral arteries from genetically hypertensive rats. *American Journal of Physiology - Heart and Circulatory Physiology* 254: 28-33
40. Fujii F, Heistad DD, Faraci FM. 1990. Ionic mechanisms in spontaneous vasomotion of the rat basilar artery in vivo. *Journal of Physiology* 430: 389-98
41. Nir Y, Mukamel R, Dinstein I, Privman E, M. H, et al. 2008. Interhemispheric correlations of slow spontaneous neuronal fluctuations revealed in human sensory cortex. *Nature Neuroscience* 11: 1100-08
42. Leopold DA, Murayama Y, Logothetis NK. 2003. Very slow activity fluctuations in monkey visual cortex: Implications for functional brain imaging. *Cerebral Cortex* 13: 422–33
43. Shmuel A, Leopold DA. 2008. Neuronal correlates of spontaneous fluctuations in fMRI signals in monkey visual cortex: Implications for functional connectivity at rest. *Human Brain Mapping* 29: 751–61
44. Kuramoto Y. 1984. *Chemical Oscillations, Waves and Turbulence*. New York: Springer Verlag
45. Munting LP, Bonnar O, Kozberg MG, Auger CA, Hirschler L, et al. 2023. Spontaneous vasomotion propagates along pial arterioles in the awake mouse brain like stimulus-evoked vascular reactivity. *Journal of Cerebral Blood Flow & Metabolism* 43: 1752-63
46. Longden TA, Dabertrand F, Koide M, Gonzales AL, Tykocki NR, et al. 2017. Capillary K^+-sensing initiates retrograde hyperpolarization to increase local cerebral blood flow. *Nature Neuroscience* 20: 717-26
47. Krolak T, Kaplan L, Navas K, Chen L, Birmingham A, et al. 2025. Brain endothelial gap junction coupling enables rapid vasodilation propagation during neurovascular coupling. *Cell* 188: 5003-19
48. Spencer NJ, Greenwood IA. 2003. Characterization of properties underlying rhythmicity in mouse portal vein. *Autonomic Neuroscience* 104: 73-82
49. Knot HJ, Nelson MT. 1998. Regulation of arterial diameter and wall [Ca^{2+}] in cerebral arteries of rat by membrane potential and intravascular pressure. *Journal of Physiology* 508: 199 –209
50. Ghosh D, Syed AU, Prada MP, Nystoriak MA, Santana LF, et al. 2017. Calcium channels in vascular smooth muscle. *Advances in Pharmacology* 78: 49-87
51. Wenceslau CF, McCarthy CG, Earley S, England SK, Filosa JA, et al. 2021. Guidelines for the measurement of vascular function and structure in isolated arteries and veins. *American Journal of Physiology: Heart and Circulation Physiology* 321: H77-H111
52. Lin LJ, Gao F, Bai YG, Bao JX, Huang XF, et al. 2009. Contrasting effects of simulated microgravity with and without daily-Gx gravitation on structure and function of cerebral and mesenteric small arteries in rats. *Journal of Applied Physiology* 107: 1710-21
53. Moshkforoush A, Ashenagar B, Harraz OF, Dabertrand F, Longden TA, et al. 2020. The capillary Kir channel as sensor and amplifier of neuronal signals: Modeling insights on K+-mediated neurovascular communication. *Proceedings of the National Academy of Sciences USA* 117: 16626-37
54. Thakore P, Alvarado MG, Ali S, Mughal A, Pires PW, et al. 2021. Brain endothelial cell TRPA1 channels initiate neurovascular coupling. *Elife* 10: e63040
55. Rosehart AC, Longden TA, Weir N, Fontaine JT, Joutel A, Dabertrand F. 2021. Prostaglandin E(2) dilates intracerebral arterioles when applied to capillaries: Implications for small vessel diseases. *Froteirs of Aging Neuroscience* 13: e695965

56. Mughal A, Nelson MT, Hill-Eubanks D. 2023. The post-arteriole transitional zone: A specialized capillary region that regulates blood flow within the CNS microvasculature. *Journal of Physiology* 601: 889-901
57. Drew PJ. 2022. Neurovascular coupling: motive unknown. *Trends in Neuroscience* 45: 809-19
58. Shih AY, Rühlmann C, Blinder P, Devor A, Drew PJ, et al. 2015. Robust and fragile aspects of cortical blood flow in relation to the underlying angioarchitecture. *Microcirculation* 22: 204-18
59. Hernández JCC, Bracko O, Kersbergen CJ, Muse V, Haft-Javaherian M, et al. 2019. Neutrophil adhesion in brain capillaries reduces cortical blood flow and impairs memory function in Alzheimer's disease mouse models. *Nature Neuroscience* 22: 413–20
60. Ji X, Zhao Y, Bai L, Wang K, Kleinfeld D. 2026. Microvascular architecture and physiological fluctuations constrain the control of cerebral microcirculation. *Proceedings of the National Academy of Sciences USA* 123: e2521872123
61. Nishimura N, Schaffer CB, Friedman B, Lyden PD, Kleinfeld D. 2007. Penetrating arterioles are a bottleneck in the perfusion of neocortex. *Proceedings of the National Academy of Sciences USA* 104: 365-70
62. Kleinfeld D, Mitra PP, Helmchen F, Denk W. 1998. Fluctuations and stimulus-induced changes in blood flow observed in individual capillaries in layers 2 through 4 of rat neocortex. *Proceedings of the National Academy of Sciences USA* 95: 15741-46
63. Giblin JT, Sreekanth Kura S, Küreli G, Jiang J, Kılıç K, et al. 2025. Brief disruptions in capillary flow result in rapid onset of hypoxia. *Neurophotonics* 12: S22803
64. Crumpler R, Roman RJ, Fan F. 2021. Capillary stalling: A mechanism of decreased cerebral blood flow in AD/ADRD. *Journal of Experimental Neurology* 2: 149-53
65. Hartmann DA, Coelho-Santos V, Shih AY. 2022. Pericyte control of blood flow across nicrovascular vones in the central nervous system. *Annual Review of Physiology* 84: 331-54
66. Ferris HR, Jeffrey DA, Guerrero MB, Birnbaumer L, Zheng F, Dabertrand F. 2025. Increased luminal pressure in brain capillaries drives TRPC3-dependent depolarization and constriction of transitional pericytes. *Science Signaling* 18: eads1903
67. Earley S. 2025. Pericytes under pressure: TRPC3 channels as gatekeepers of capillary flow. *Science Signaling* 18: eadw7185
68. Hladky SB, Barrand MA. 2022. The glymphatic hypothesis: The theory and the evidence. *Fluids and Barriers of the CNS* 19: e282
69. Rasmussen MK, Mestre H, Nedergaard M. 2011. Fluid transport in the brain. *Physiological Reviews* 103: 1025-151
70. Bohr T, Hjorth PG, Holst SC, Hrabětová S, Kiviniemi V, et al. 2022. The glymphatic system: Current understanding and modeling. *iScience* 25: e104987
71. Kipnis J, Benveniste H, Eichmann A, Thomas J-L, Reich DS, et al. 2025. Resolving the mysteries of brain clearance and immune surveillance. *Neuron* 113: 3908-23
72. Diem AK, M. SM, Gatherer M, Bressloff NW, Carare RO, Richardson G. 2017. Arterial pulsations cannot drive Intramural periarterial drainage: Significance for Aβ drainage. *Frontiers of Neuroscience* 11: e475
73. Kedarasetti RT, Drew PJ, Costanzo F. 2020. Arterial pulsations drive oscillatory flow of CSF but not directional pumping. *Scientific Reports* 10: e10102
74. Aldea R, Weller RO, Wilcock DM, Carare RO, Richardson G. 2019. Cerebrovascular smooth muscle cells as the drivers of intramural periarterial drainage of the brain. *Frontiers in Aging Neuroscience* 11: e1
75. Kedarasetti RT, Drew PJ, Costanzo F. 2022. Arterial vasodilation drives convective fluid flow in the brain: a poroelastic model. *Fluids and Barriers of the CNS* 19: e34

76. Gan Y, Holstein-Rønsbo S, Nedergaard M, Boster KAS, Thomas JH, Kelley DH. 2023. Perivascular pumping of cerebrospinal fluid in the brain with a valve mechanism. *Journal of the Royal Society Interface* 20: e20230288
77. Garborg CS, Ghitti B, Zhang Q, Ricotta JM, Frank N, et al. 2026. Gut-brain hydraulics: Brain motion and CSF circulation is driven by mechanical coupling. *Nature Neuroscience* 29
78. Asgari M, de Zélicourt DA, Kurtcuoglu V. 2016. Glymphatic solute transport does not require bulk flow. *Scientific Reports* 6: e38635
79. Aspelund A, Antila S, Proulx ST, Karlsen TV, Karaman S, et al. 2015. A dural lymphatic vascular system that drains brain interstitial fluid and macromolecules. *Journal of Experimental Medicine* 212: 991–99
80. Zhang Q, Niu Y, Li Y, Xia C, Chen Z, et al. 2025. Meningeal lymphatic drainage: Novel insights into central nervous system disease. *Signal Transduction and Targeted Therapy* 10: e142
81. Koh L, Zakharov A, Johnston M. 2005. Integration of the subarachnoid space and lymphatics: is it time to embrace a new concept of cerebrospinal fluid absorption? *Cerebrospinal Fluid Research* 2: e6
82. Melin E, Eide PK, Ringstad G. 2020. In vivo assessment of cerebrospinal fluid efflux to nasal mucosa in humans. *Science Reports* 10: e14974
83. Iliff JJ, Wang M, Liao Y, Plogg BA, Peng W, et al. 2012. A paravascular pathway facilitates CSF flow through the brain parenchyma and the clearance of interstitial solutes, Including amyloid **β**. *Science Translational Medicine* 4: e111
84. Albargothy NJ, Johnston DA, MacGregor-Sharp M, Weller RO, Verma A, et al. 2018. Convective influx/glymphatic system: tracers injected into the CSF enter and leave the brain along separate periarterial basement membrane pathways. *Acta Neuropathologica* 136: 139–52
85. Jiang-Xie L-F, Drieu A, Bhasiin K, Quintero D, Smirnov I, Kipnis J. 2024. Neuronal dynamics direct cerebrospinal fluid perfusion and brain clearance. *Nature* 627: 157–64
86. Chayama Y, Rao NR, Perla D, Zhang Z, Reid M, et al. 2026. Physiological brain clearance architecture revealed by neuronal protein tracing. *Cell* 189: 1-19
87. van Veluw SJ, Hou SS, Calvo-Rodriguez M, Arbel-Ornath M, Snyder AC, et al. 2020. Vasomotion as a driving force for paravascular clearance in the awake mouse brain. *Neuron* 105: 549-61
88. Hauglund NL, Andersen M, Tokarska K, Radovanovic T, Kjaerby C, et al. 2025. Norepinephrine-mediated slow vasomotion drives glymphatic clearance during sleep. *Cell* 188: 606-22
89. Mestre H, Tithof J, Du T, Song W, Peng W, et al. 2018. Flow of cerebrospinal fluid is driven by arterial pulsations and is reduced in hypertension. *Nature Communications* 9: e4878
90. Zong X, Kim T, Kim S-G. 2012. Contributions of dynamic venous blood volume versus oxygenation level changes to BOLD fMRI. *NeuroImage* 60: 2238–46
91. Holstein-Rønsbo S, Gan Y, Giannetto MJ, Rasmussen MK, Sigurdsson B, et al. 2023. Glymphatic influx and clearance are accelerated by neurovascular coupling. *Nature Neuroscience* 26: 1042-53
92. Choi S, Cheol-Jang D, Chung G, Kim SK. 2022. Transcutaneous auricular vagus nerve stimulation enhances cerebrospinal fluid circulation and restores cognitive function in the rodent model of vascular cognitive impairment. *Cells* 11: e11193019
93. Xie L, Kang H, Xu Q, Chen MJ, Liao Y, et al. 2013. Sleep drives metabolite clearance from the adult brain. *Science* 342: 373-77
94. Bojarskaite L, Vallet A, Bjørnstad DM, Gullestad Binder KM, Cunen C, et al. 2023. Sleep cycle-dependent vascular dynamics in male mice and the predicted effects on perivascular cerebrospinal fluid flow and solute transport. *Nature Communications* 14: 953
95. Miao A, Luo T, Hsieh B, Edge CJ, Gridley M, et al. 2024. Brain clearance is reduced during sleep and anesthesia. *Nature Neuroscience* 27: 1046–50

96. Agarwal N, Lewis, L. D., Hirschler L, ., Rivera LR, Naganawa S, et al. 2013. Current understanding of the anatomy, physiology, and magnetic resonance imaging of neurofluids: Update from the 2022 "ISMRM Imaging Neurofluids Study group" Workshop in Rome. *Journal of Magnetic Resonant Imaging* 59: 431-49

97. Fultz NE, Bonmassar G, Setsompop K, Stickgold RA, Rosen BR, et al. 2019. Coupled electrophysiological, hemodynamic, and cerebrospinal fluid oscillations in human sleep. *Science* 366: 628-31

98. Hirschler L, Runderkamp BA, Decker A, van Harten TW, Scheyhing P, et al. 2025. Region-specific drivers of CSF mobility measured with MRI in humans. *Nature Neuroscience* 28: 2392-401

99. Erhardt EB, Mayer AR, Lin HC, PIrio-Richardson SE, Shaff NA, et al. 2025. The influence of intermittent hypercapnia on cerebrospinal fluid flow and clearance in Parkinson's disease and healthy older adults. *Nature Partner Journal Parkinson's Disease* 11: 334

100. Greenberg SM. 2026. Cerebral amyloid angiopathy. *New England Journal of Medicine* 394: 1836-45

101. Greenberg SM, Bacskai BJ, Hernandez-Guillamon M, Pruzin J, Sperling R, van Veluw SJ. 2020. Cerebral amyloid angiopathy and Alzheimer disease - one peptide, two pathways. *Nature Reviews of Neurology* 16: 30-42

102. Shin HK, Jones PB, Garcia-Alloza M, Borrelli L, Greenberg SM, et al. 2007. Age-dependent cerebrovascular dysfunction in a transgenic mouse model of cerebral amyloid angiopathy. *Brain*: 2310-19

103. Koemans EA, Chhatwal JP, van Veluw SJ, van Etten ES, van Osch MJP, et al. 2023. Progression of cerebral amyloid angiopathy: a pathophysiological framework. *Lancet Neurology* 22: 632-42

104. Dumas A, Dierksen GA, Gurol ME, Halpin A, Martinez-Ramirez S, et al. 2012. Functional magnetic resonance imaging detection of vascular reactivity in cerebral amyloid angiopathy. *Annals of Neurology* 72: 76-81

105. Peca S, McCreary CR, Donaldson E, Kumarpillai G, Shobha N, et al. 2013. Neurovascular decoupling is associated with severity of cerebral amyloid angiopathy. *Neurology* 81: 1659-65

106. van Opstal AM, van Rooden S, van Harten T, Ghariq E, Labadie G, et al. 2017. Cerebrovascular function in presymptomatic and symptomatic individuals with hereditary cerebral amyloid angiopathy: a case-control study. *Lancet Neurology* 16: 115-22

107. Mughal A, Harraz OF, Gonzales AL, Hill-Eubanks D, Nelson MT. 2021. PIP2 improves cerebral blood flow in a mouse model of Alzheimer's disease. *Function* 2: zqab010

108. Kozberg MG, Munting LP, Hanlin LH, Auger CA, van den Berg ML, et al. 2025. Vasomotion loss precedes impaired cerebrovascular reactivity and microbleeds in cerebral amyloid angiopathy. *Brain Communications* 7: e186

109. Kim SH, Ahn JH, Yang H, Lee P, Koh GY, Jeong Y. 2020. Cerebral amyloid angiopathy aggravates perivascular clearance impairment in an Alzheimer's disease mouse model. *Acta Neuropathologica Communications* 8: 181

110. Chen X, Liu X, Koundal S, \Elkin R, Zhu X, et al. 2022. Cerebral amyloid angiopathy is associated with glymphatic transport reduction and time-delayed solute drainage along the neck arteries. *Nature Aging* 2: 214-23

111. Robbins EM, Betensky RA, Domnitz SB, Purcell SM, Garcia-Alloza M, et al. 2006. Kinetics of cerebral amyloid angiopathy progression in a transgenic mouse model of Alzheimer disease. *Journal of Neuroscience* 11: 365-71

112. Drew PJ, Shih AY, Driscoll JD, Knutsen PM, Davalos D, et al. 2010. Chronic optical access through a polished and reinforced thinned skull. *Nature Methods* 7: 981-84

113. Shih AY, Mateo C, Drew PJ, Tsai PS, Kleinfeld D. 2012. A polished and reinforced thinned skull window for long-term imaging and optical manipulation of the mouse cortex. *Journal of Visualized Experiments*: www.jove.com/video/3742

114. Akata T, Warltier DC. 2007. General anesthetics and vascular smooth muscle: Direct actions of general anesthetics on cellular mechanisms regulating vascular tone. *Anesthesiology* 106: 365-91

115. Kwong KK, Belliveau KW, Chesler DA, Goldberg IE, Weisskoff RM, et al. 1992. Dynamic magnetic resonance imaging of human brain activity during sensory stimulation. *Proceedings of the National Academy of Sciences USA* 89: 5675-79

116. Tønnesen J, KrishnaInavalli VVG, Nägerl V. 2018. Super-resolution imaging of the extracellular epace in living brain tissue. *Cell* 172: 1108-21

117. Iliff JJ, Wang M, Zeppenfeld DM, Venkataraman A, Plog BA, et al. 2013. Cerebral arterial pulsation drives paravascular CSF–interstitial fluid exchange in the murine brain. *Journal of Neuroscience* 33: 18190-99

118. Badea A, Ali-Sharief AA, Johnson GA. 2007. Morphometric analysis of the C57BL/6J mouse brain. *NeuroImage* 37: 683 – 93

119. Varadarajan D, Hu Z, Gomez DEP, Proulx S, Wighton P, et al. 2025. Separating vessel diameter, blood velocity and oxygenation responses to activation: joint magnitude-phase analysis of phase-contrast. *Proceedings of the International Society for Magnetic Resonance in Medicine* 33: e1439

120. Proulx S, Varadarajan D, Duckworth J, Hu Z, Chen J, et al. 2025. *Contrast mechanisms in vessel-scale human fMRI: Ultra-slow post-stimulus “ringing” oscillations in cortical arteries*. Presented at International Society for Magnetic Resonance in Medicine Annual Meeting, Honolulu, Hawai'i

Figure 1. Phenomenology of vasomotion as observed with optical tools in the neocortex of mouse. (**a**) Set-up with head-fixed awake mouse. A window above a thin skull provides access for imaging into brain of one or both hemispheres, concurrent with measurements of local field potential (LFP) across selected regions. Panel adapted with permission from Reference 23; copyright 2017 Elsevier. (**b**) In vivo two-photon laser scanning microscopy (TPLSM) imaging of vasomotion in pial arterioles across both hemispheres; blood plasma is stained with fluorescein-dextran to permit measurements of diameter. Shown is the maximally projected image stack across 500-μm of the preparation. An arbitrary-line-scan path (yellow for acquisition segments) spans both hemispheres. The expanded images are single planes in each hemisphere and highlight the path of the line-scan through individual vessels whose diameters were concurrently monitored. Panels b-d adapted with permission from Reference 28, copyright 2015 Optica Publishing Group. (**c**) Vasomotion oscillations measured simultaneously from pial arteries in the right (green) and left (red) hemispheres of panel b. (**d**) Magnitude of the spectral coherence between the two arterioles as calculated from 540 s traces and a bandwidth (full-width-at-half-maximum amplitude) of 0.04 Hz. (**e**) Coupled oscillator model for vasomotion. Variations in gamma-band electrical power leads to partial entrainment of the vasomotion oscillations in the smooth muscle of cortical arterioles. Increases in neuronal activation, in turn, dilates the arterioles and leads to an increase in the supply of fresh blood, as measured by a positive change in the blood oxygenation level dependent functional magnetic resonant Imaging (BOLD fMRI) signal. Abbreviation: cerebral blood volume functional magnetic resonant Imaging (CBV fMRI). Panel adapted with permission from Reference 23, copyright 2017 Elsevier. (**f**) Two-photon image showing labeling for concurrent measurements of both arteriole diameter, with plasma labeled with Cy5-dextran, and arteriole activation, with the genetically encoded calcium indicator GCaMP-8 expressed in arteriole smooth muscles. Panels f-k adapted with permission from Reference 30, copyright 2024 Elsevier. (**g**) Spectrogram from concurrent measurements of arteriole diameter and smooth muscle calcium. (**h**) Short-term spectral power and coherence from two, 100 s periods in panel g. (**i**) Distribution of peak vasomotion frequency from a cohort of 8,869 pial vessels across 24 mice. (**j**) Phase portraits of the dominant space-frequency mode of widefield images of cortex at the vasomotion frequency for an example resting-state trial; data obtained from arteriole GCaMP imaging data. Rostral is up and delay increases with increasing phase. (**k**) Model of pial and penetrating vessel traveling waves. The observed vasodynamics are influenced by both ongoing neuronal activity and neighboring

smooth muscle cell oscillators. Vascular phase, partially driven by neuronal activity, progresses over millimeter scales but is variable on shorter length scales to potentially form constant-phase parcels.

Figure 2. Phenomenology of vasomotion relative to neuronal drive for neocortex of mouse. (**a**) Example trace of local field potential (LFP) and the time series of both the integrated gamma-band power in the LFP and diameter for one arteriole in the field. Panel adapted with permission from Reference 23, copyright 2017 Elsevier. **(b**) Scatterplot of pial arteriole phase gradient versus neuronal envelope phase gradient. Arterioles whose vessel and neuronal waves travel in the same direction have same-signed $\mathbf{k}_{vaso}$ and $\mathbf{k}_{neural}$ (red points). Points with $\mathbf{k}_{vaso} = \mathbf{k}_{neural}$ represent waves that travel in the same direction with equal speeds. Insert shows the connected correlation, plotted cumulatively for all $|\mathbf{k}| = (k^2_{neural} + k^2_{vaso})^{1/2}$; standard error is shown in gray. Adapted with permission from Reference 30; copyright 2024 Elsevier. **(c)** Magnitude coherence between arteriole diameter, via the genetically encoded calcium indicator GCaMP expressed in arteriole smooth muscle cells (SMCs), and neuronal envelope, via the genetically encoded calcium indicator jRGECO1a expressed in vibrissa cortical excitatory neurons, during air puff stimulation. Adapted with permission from (30). Note the slight shift in coherence during vibrissa stimulation. Panels b and c adapted with permission from Reference 30; copyright 2024 Elsevier. **(d)** Time series of arteriole diameter (red) and gamma-band power (green) from optogenetically driving L5b neurons with light pulses modulated by 10 s sinusoidal envelope (blue); note driven vasodilation. The lower trace is an expanded view. Set-up as in panel a with addition of epi-illumination with 445 nm laser light concurrent with two-photon laser scanning microscopy (TPLSM) imaging. Panel adapted with permission from Reference 23; copyright 2017 Elsevier.

Figure 3. High-gain electromechanical coupling amplifies capillary-initiated hyperpolarizing signals into arteriolar dilation. Shaded regions in panels a–c denotes the high-gain physiological range in which small electrical signals are converted into disproportionately large changes in $[Ca^{2+}]$ and diameter. (**a**) Sigmoidal relationship between smooth muscle cell (SMC) membrane potential (E_M) and global intracellular $[Ca^{2+}]$, illustrating the steep voltage dependence of Ca^{2+} entry over the physiological operating range. The red

point marks a representative resting state, and a ~ 5-mV hyperpolarization is predicted to reduce global SMC [Ca^{2+}] by ~ 30 nM. (**b**) Composite relationship between SMC E_M and arterial diameter, showing that a ~ 5-mV hyperpolarization is sufficient to produce an ~ 20 % dilation. (**c**) Inverse sigmoidal relationship between SMC [Ca^{2+}] and arterial diameter, indicating that a ~ 30 nM reduction in global SMC [Ca^{2+}] is sufficient to generate an ~ 20 % dilation. (**d**) Schematic of the experimental paradigm in which local K^+ application to the capillary bed is used to evoke upstream vasodilatory responses. Panels d-f adapted with permission from Reference 87; copyright 2020 Elsevier. (**e**) Representative image of the stimulating pipette positioned adjacent to capillaries. (**f**) Example trace showing dilation of an upstream arteriole in response to brief K^+ (10 mM) pulses applied to capillaries. (**g**) Working model in which slow fluctuations in gamma-band power increase extracellular K^+, activate capillary K_{IR} channels, and generate conducted hyperpolarizing signals that hyperpolarizes SMCs, lowers intracellular [Ca^{2+}], and produces dilation.

Figure 4. Low frequency stimulation entrains vasomotion and promotes clearance of exogenous tracers in the mouse brain. (**a**) Schematic illustration of an awake mouse receiving visual, vibrissa, or optogenetic stimulation to drive vasomotion. Created in BioRender. (**b**) Schematic illustration of vasodilation during stimulation, coinciding with a narrowing of the perivascular space. Created in BioRender. (**c**) Representative example of an arteriole (art.) and a venule (ven.) captured with in vivo two-photon laser scanning microscopy (TPLSM) in an unanesthetized head-fixed mouse with a chronic cranial window over the right visual cortex. Fluorescein dextran was injected intravenously to label the vessel lumens. Panels c-h adapted with permission from Reference 87; copyright 2020 Elsevier. (**d**) Representative example of the change in diameter of a single arteriole measured with in vivo TPLSM; region of interest (ROI) indicated in panel c. Low frequency visual stimulation (0.05 Hz) was found to entrain vasomotion at the stimulation frequency. Grey bar = visual stimulation ON, white bars = visual stimulation OFF. (**e**) A peak at the stimulation frequency was observed in the plot of spectral power density. (**f**) Representative example of measuring signal decay in the perivascular space of a pial surface arteriole, as a proxy for perivascular clearance. A fluorescently-labeled exogenous tracer, i.e., 70 kDa dextran, which was injected intravenously prior to imaging, was released into the subarachnoid space with laser irradiation of a nearby venule (arrow). (**g**) The fluorescent signal decay measured along the pial surface arterioles (ROI indicated in panel f) was found to

be correlated with the amplitude of vasomotion. (**h**) Low frequency visual stimulation (0.05 Hz) resulted in faster clearance of the tracer. (**i**) Representative example of measuring signal decay along the middle cerebral artery with wide-field optical microscopy. A fluorescently-labeled exogenous tracer was injected into the cisterna magna and allowed to circulate for 30-minutes prior to imaging. Panels i and j adapted with permission from Reference 91; copyright 2023 Springer Nature. (**j**) Low frequency unilateral vibrissa stimulation (0.01 Hz) in ketamine/xylazine anesthetized mice, resulted in faster clearance of tracer from the stimulated hemisphere.

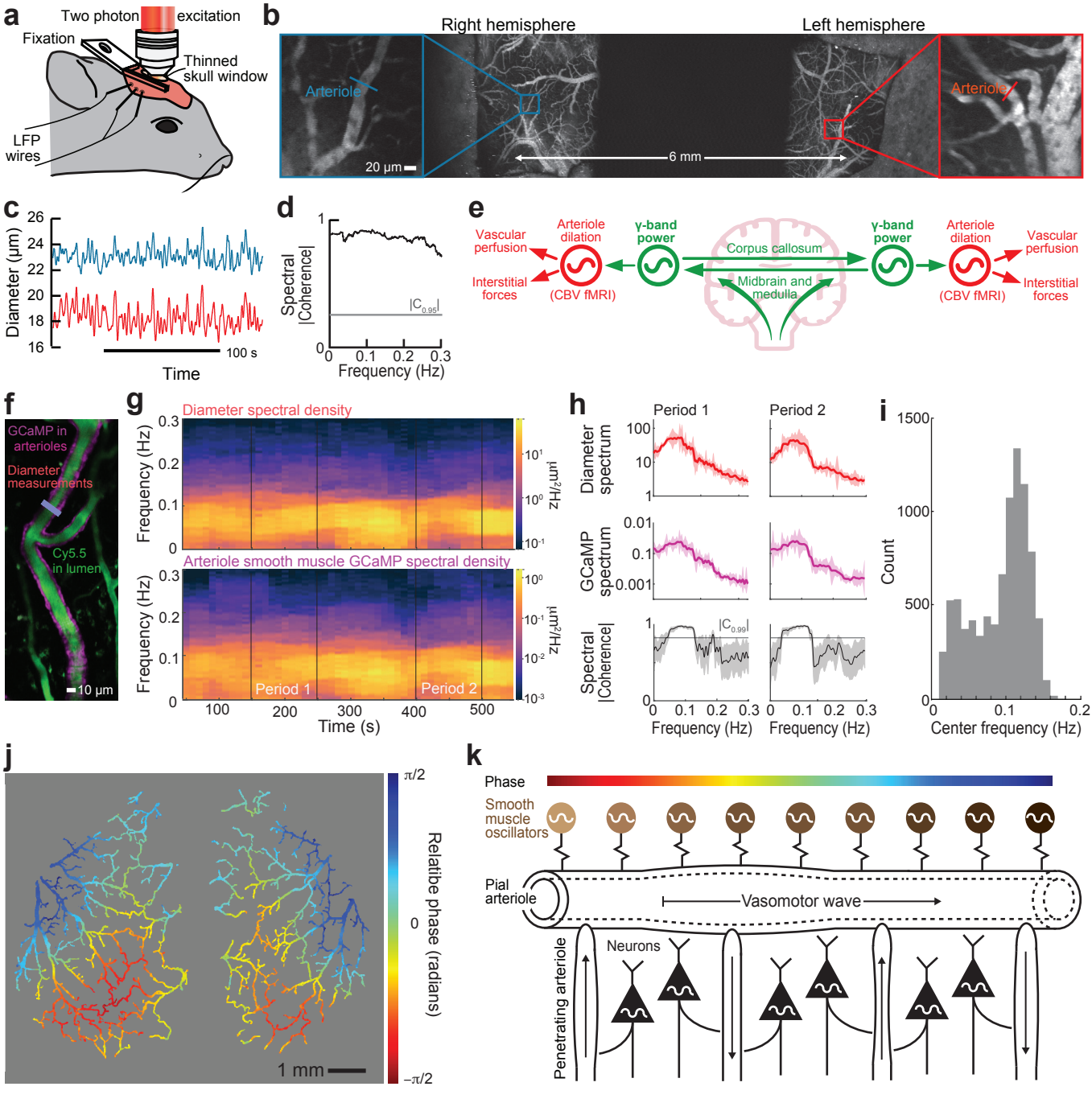

Figure 1. Earley, Kleinfeld and Van Veluw.

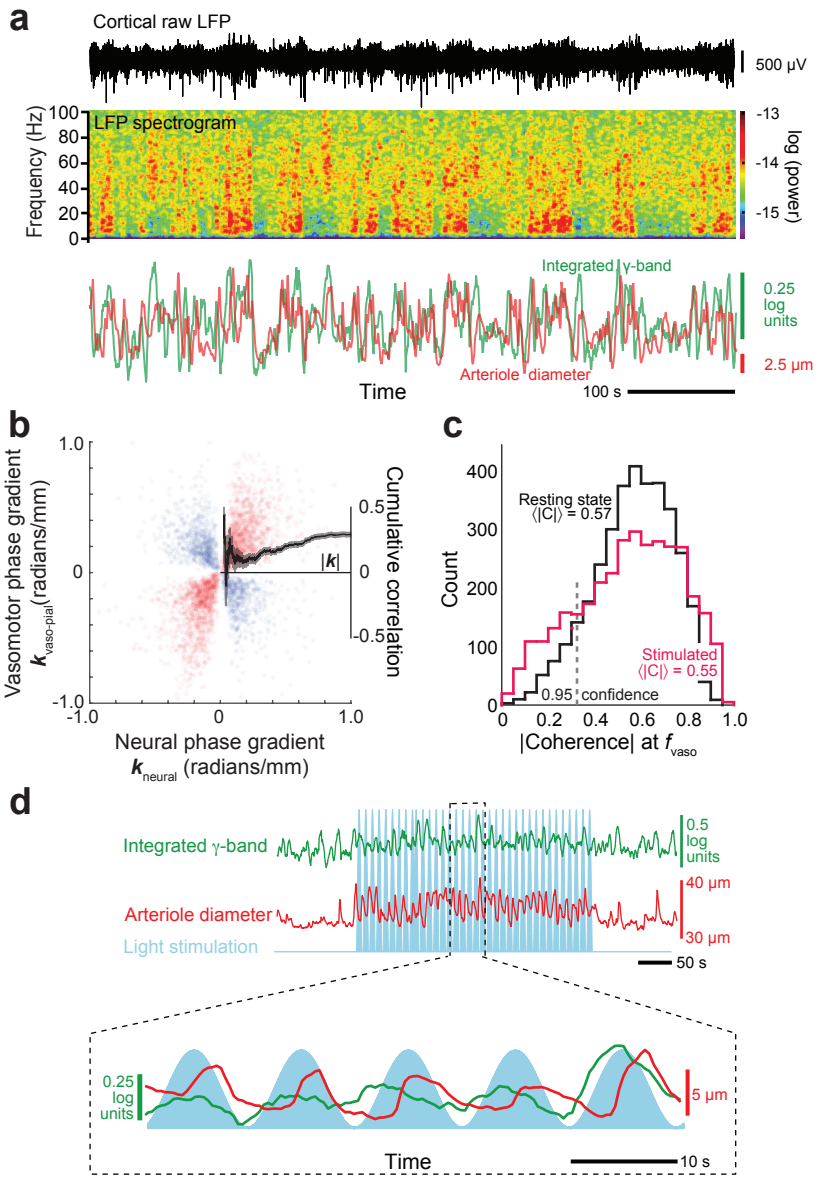

Figure 2. Earley, Kleinfeld and Van Veluw.

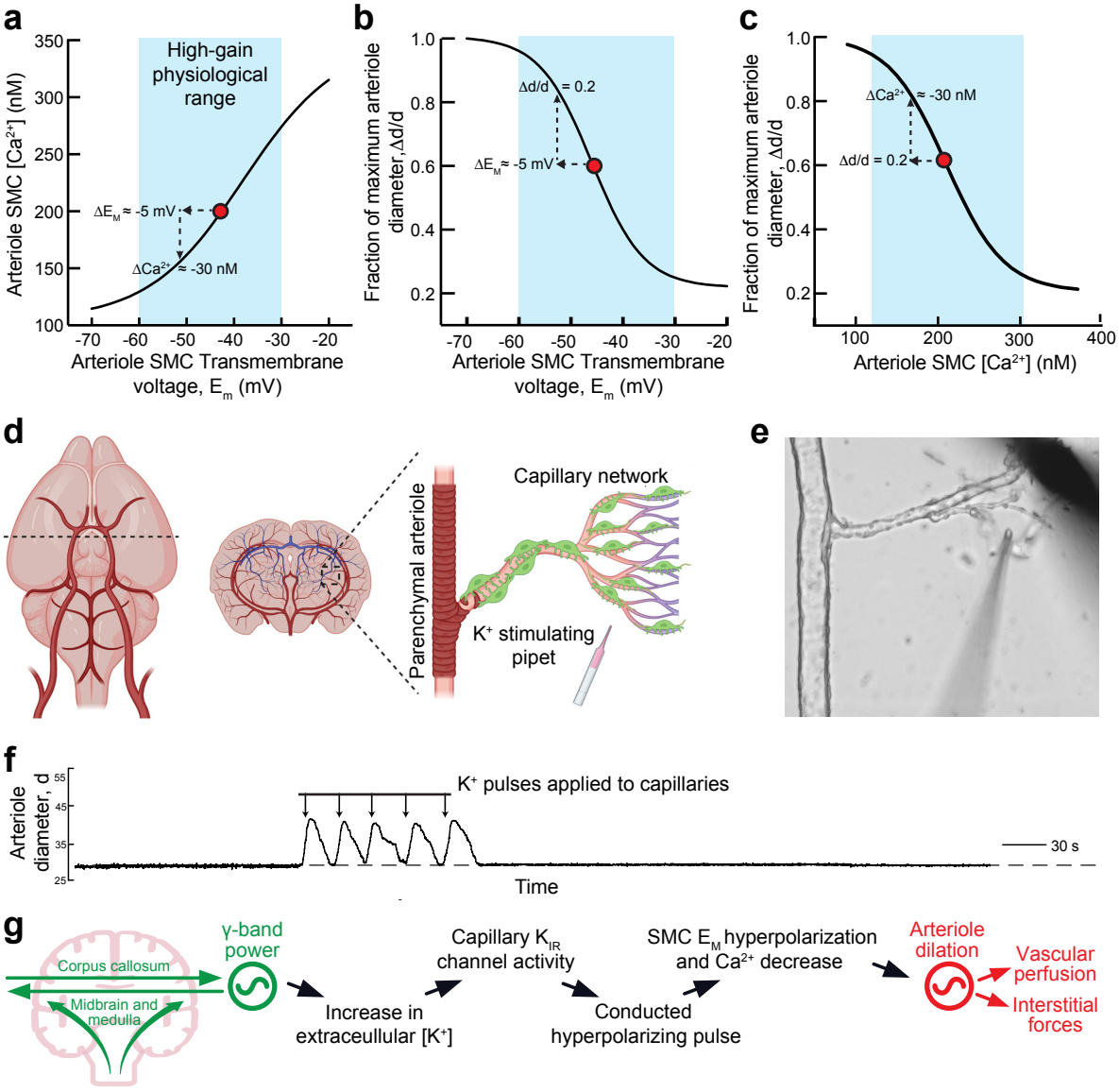

Figure 3: Earley, Kleinfeld, and Van Veluw

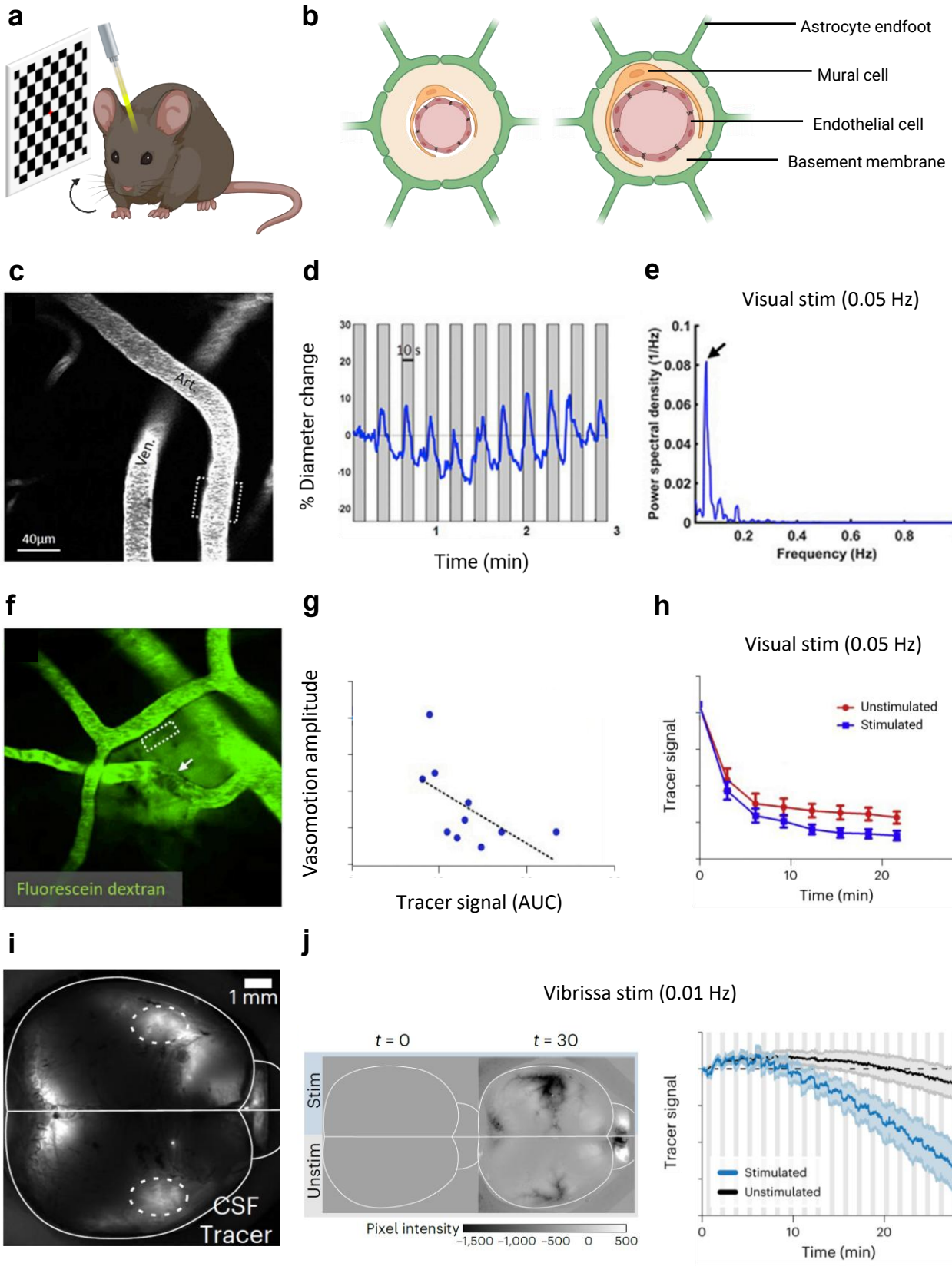

Figure 4: Earley, Kleinfeld, and Van Veluw